Mixing of a two-phase fluid by cavity flow

Ravi Chella[1] and Jorge Viñals[1,2]
[1] *Department of Chemical Engineering, Florida A&M University/Florida State University, College of Engineering, Tallahassee, Florida 32310*
[2] *Supercomputer Computations Research Institute, Florida State University, Tallahassee, Florida 32306-4052*
(Received 9 August 1995)

Interface stretching during mixing of a two-phase fluid in shear flow is investigated numerically by introducing a mesoscopic description of the fluid. The classical infinitely thin boundary of separation between the two phases is replaced by a transition region of small but finite width, across which the order parameter of the two-phase fluid changes continuously. We consider the case of a conserved scalar order parameter and a fluid velocity that satisfies a modified Navier-Stokes equation that includes an explicit coupling term to the order parameter. In the macroscopic limit of a very thin interface, this coupling term gives rise to capillary forces. We focus on the limit of low Reynolds number flow and compute the interface stretching as a function of time for a range of parameters of the fluid. At early times and small coupling, our calculation agrees with the classical case of a material line passively advected by the flow. At later times, the interface stretching is seen to reach a maximum as capillary forces and diffusive relaxation of the order parameter become dominant.

PACS number(s): 68.10.−m, 82.20.Wt, 05.70.Ln, 47.11.+j

I. INTRODUCTION

We present a computational approach, based on a mesoscopic description of a two-phase fluid, to study the motion of an active interface that separates two coexisting fluid phases when the flow is driven by an externally imposed shear stress. The configuration considered here is that of cavity flow, a widely studied case that approximates the mixing conditions found during extrusion [1].

The classical mathematical description of multiphase flows involves the solution of a moving boundary problem. In it, the equations governing fluid motion are solved inside each phase, subject to boundary conditions on the moving interface. In the particular case in which the two phases are being mixed by the action of an imposed flow, the spatial regions occupied by either phase are deformed, the amount of interface area per unit volume increases with time (interface stretching), and the characteristic length scale of the resulting microstructure decreases. Under these conditions, a numerical solution of the coupled equations governing fluid flow and interface motion becomes extremely complex.

The method described in this paper applies to both passive and active interfaces, although we focus mostly on the latter case. A passive interface separates two similar fluids and has negligible interfacial tension. Hence the interface is convected by the flow without affecting it. If interdiffusion is also negligible, any material region stretches and folds by the action of the flow. If interdiffusion is not negligible, any sharp interface between the two phases becomes progressively diffuse and the extent of mixing of the two phases has to be characterized not only by the interface stretching but by the spreading of the level sets of the composition field as well. A moving active interface, on the other hand, modifies the flow through capillary effects. Furthermore, as the characteristic length scale of the resulting microstructure during mixing becomes smaller and smaller, surface tension effects become dominant leading in some cases to domain breakup.

We introduce in this paper a computational method to study the motion of an initially flat interface that separates two coexisting thermodynamic phases, under the action of an externally imposed shear flow. We aim at describing microstructure evolution during mixing in terms of the amount of interface area per unit volume of the fluid and of the geometrical shape and distribution of the domains of the two phases. The basic idea underlying the method is to replace the dividing surface between the two coexisting phases by a transition region of small but finite width, across which the various thermodynamic variables change continuously. Thus the original moving boundary problem is replaced by an ordinary system of partial differential equations, with solutions that are continuous throughout the system but have large variations in the interfacial region.

Our approach follows the same general principles as Ginzburg-Landau models of phase separation [2], phase field models of solidification [3–7], and various phenomenological models used to study the decay of fluctuations at a critical point [8]. The model that we study was originally introduced to analyze the relaxation of critical fluctuations in simple or binary fluids (model H) [8,9] and critical fluctuations of fluids [10,11] or polymers under shear [12]. We focus here on a different region of parameters (away from any critical point), such that there are large regions of space in which the order parameter $\phi(\vec{r},t)$ is almost uniform (bulk phases), separated by interfacial regions of small width ξ, over which the order parameter changes continuously. Additional previous work in this region of parameters includes the study of hydrodynamic effects during spinodal decomposition in a binary fluid

 ©1996 The American Physical Society

[13,14]. We finally note that the model equations that we use below can be derived by following the methods of continuum mechanics [15].

Moving boundary problems arise in a variety of disciplines such as combustion, multiphase flows, and crystal growth. Analytic solutions are rare and a large number of computational approaches have been developed (a review of the general ideas behind the various methods can be found in Refs. [16,17]). Hyman [16], for example, has divided interfacial tracking methods into surface tracking, volume tracking, and moving mesh methods. In surface tracking methods, the interface location and motion are defined by the position and motion of a number of "marker particles," which are advected by the flow without modifying it. Surface tracking methods often fail when there are changes in the topology of the interface (such as the reconnections that appear during coalescence) or when noncontiguous elements of the interface become too close to each other. The most often used volume tracking methods are the so-called "volume of fluid" (VOF) methods [16,18–21]. These are generalizations of the marker and cell method in which marker particles are replaced by a function, called the fractional volume of fluid function, that is discontinuous at the interface and is passively advected by the flow. Recent extensions of these methods involve the introduction of a color or indicator function [19–21] that changes continuously across the interface. In effect, the mathematical boundary of separation between the two fluids is replaced by a transition region of small but finite width. Further extensions have incorporated capillary forces as body forces in the Navier-Stokes equation and thus active interfaces have been considered. From a computational standpoint, the approach that we follow in this paper is very similar to these latter methods. However, there are two important differences. First, the order parameter (which plays a role analogous to a color function in terms of distinguishing the two coexisting phases) does have a physical meaning: it is a thermodynamic variable upon which the free energy of the system depends. As a consequence, and in contrast to VOF methods, the surface tension of the interface is not an independent parameter, but is determined by this same free energy. The second difference is that the equation being solved for the color function $C(\vec{r},t)$ in VOF methods is

$$\frac{\partial C}{\partial t}+\vec{v}\cdot\vec{\nabla}C=0. \tag{1}$$

Differential velocities across the smeared interface result in an artificial broadening of the interfacial region as a function of time. To compensate for this problem, the color function is continually redistributed around the new location of the interface in some predefined way that depends on the particular algorithm being employed. In our method, the relaxation of the order parameter field is driven by local minimization of the free energy. This ensures that the transition region separating the two bulk phases retains its integrity throughout the calculation.

Finally, in moving mesh methods the two bulk phases are discretized into elements such that the interface coincides with element boundaries. In problems in which large deformations of the interface occur, frequent remeshing is required, rendering the method impractical. Also for active interfaces, special treatment is necessary because of the multivaluedness of the pressure at the interfacial nodal points.

Previous numerical work on mixing of fluids by cavity flow was done by Bigg and Middleman [22]. They used the marker-and-cell method to track the evolution of the interface between fluids of differing viscosities. However, their calculations did not take surface tension into account and were carried out only for relatively small values of the interfacial stretch S [$S/S(t=0)<5$]. The calculations that we report below reach values as high as $S/S(t=0)=20$.

We present in Sec. II the model used and some of its properties and in Sec. III the numerical algorithm used. Section IV presents the results of our calculations of the interface stretching as a function of time, as well as its dependence on the various parameters of the fluid.

II. MODEL EQUATIONS

Consider a two-dimensional square cavity of side L, enclosing an incompressible, Newtonian two-phase fluid. Let ϕ be the order parameter appropriate for the two thermodynamic phases in question. Well within the bulk phases, $\phi(\vec{r},t)=\phi_{\pm}$, with $\phi_{\pm}$ the two equilibrium values of the order parameter across a flat interface at the temperature considered as dictated by minimization of the free energy of the system $\mathcal{F}$.

As discussed in the Introduction, in order to determine the kinetic equation obeyed by ϕ, as well as its coupling to the Navier-Stokes equation, we borrow from previous studies of critical phenomena and phase separation in binary systems. Since the description we use retains physical processes occurring at the length scale of the thickness of the interface between the two phases, these processes have to be explicitly modeled. At present, there are no rigorous theories that describe dissipative processes at that scale and therefore we follow the conventional approach that involves introducing a phenomenological free-energy density that includes terms proportional to the gradient of the order parameter. In studies of phase separation in binary fluids, $\mathcal{F}$ is normally approximated by the Cahn-Hilliard free energy [23]. For an isothermal binary system, the free energy per unit volume depends on the total mass density ρ, temperature, and, for example, the density of one of the species ρc, where c is the (dimensionless) mass fraction, which plays the role of the order parameter (denoted by ϕ in the text). Due to the large changes in order parameter in the interfacial region, one introduces a modification of the local thermodynamic equilibrium free energy by introducing an explicit dependence of the free-energy density on the gradient of the order parameter. However, typical density variations are on scales large compared with the thickness of the interfacial region and a square gradient contribution for the total mass density is not required. If, for example, one

would use this formalism to study polymer solutions, $\mathcal{F}$ would be the Flory-Huggins free energy instead [24,25].

In what follows, we consider an order parameter that satisfies a local balance equation

$$\frac{\partial \phi}{\partial t} + \vec{\nabla} \cdot (\phi \vec{v}) + \vec{\nabla} \cdot \vec{J} = 0, \tag{2}$$

where $\vec{v}$ is the local velocity of an element of fluid and $\vec{J}$ is the dissipative flux of ϕ. A constitutive equation for $\vec{J}$ is then introduced in the usual fashion

$$\vec{J} = -M \vec{\nabla} \mu. \tag{3}$$

The coefficient M is a mobility or Onsager coefficient of microscopic origin, which in a binary fluid, for example, can be calculated from measurements of the mutual diffusion coefficient and of the order parameter susceptibility away from the critical point. μ is the chemical potential conjugate to the order parameter $\mu = \delta \mathcal{F} / \delta \phi(\vec{r}, t)$, where $\delta / \delta \phi(\vec{r}, t)$ stands for variational derivative with respect to ϕ. This generalization of the definition of the chemical potential is necessary since $\mathcal{F}$ depends explicitly not only on ϕ but on its gradient as well. In what follows, we restrict our calculations to the Cahn-Hilliard free energy, so that the chemical potential μ is given by [23,8]

$$\mu = \delta \mathcal{F} / \delta \phi(\vec{r}, t) = -K \nabla^2 \phi - r \phi + u \phi^3, \tag{4}$$

where K, r, and u are three positive constants. Equilibrium solutions are given by minimization of $\mathcal{F}$ with respect to ϕ [$\mu = 0$ in Eq. (4)]. One finds two stable uniform solutions given by $\phi_+ = \sqrt{r/u}$ and $\phi_- = -\sqrt{r/u}$, representing bulk coexisting phases, and a one-dimensional (say, along the z direction) nonuniform solution $\phi_0(z) = \phi_+ \tanh z / \sqrt{2} \xi$ that satisfies the boundary conditions $\phi_0(z \to \pm \infty) = \phi_\pm$. This solution describes a planar interface normal to the z direction of thickness $\xi = \sqrt{K/r}$ that separates the two bulk phases.

Equations (2)–(4) have to be supplemented with an equation governing fluid flow. In the case of an incompressible and Newtonian fluid, we consider the Navier-Stokes equation, generalized to allow for an explicit coupling to the order parameter ϕ [8,13,15],

$$\vec{\nabla} \cdot \vec{v} = 0, \tag{5}$$

$$\rho \left[\frac{\partial \vec{v}}{\partial t} + \left(\vec{v} \cdot \vec{\nabla} \right) \vec{v} \right] = -\vec{\nabla} p + \vec{\nabla} \cdot (2 \eta D) + \mu \vec{\nabla} \phi, \tag{6}$$

where p is the pressure, ρ and η are the density and shear viscosity of the fluid, and $D = (\vec{\nabla} \vec{v} + \vec{\nabla} \vec{v}^T)/2$ is the symmetric part of the velocity gradient tensor. In this model, the density and shear viscosity of both phases are equal.

We now briefly review the limit $\xi \kappa \to 0$ of Eqs. (2)–(6) (see also Ref. [13]). Far away from interfaces, an outer solution can be found by linearizing Eqs. (2)–(4) around the bulk equilibrium solution. This procedure yields the standard convection-diffusion equation with diffusivity $2Mr$. Boundary conditions for the outer solution at two-phase interfaces follow from the local conservation law [Eqs. (2) and (3)] $\Delta \phi \, (\vec{u} - \vec{v}) \cdot \hat{\vec{n}} = -M [\vec{\nabla} \mu_+ - \vec{\nabla} \mu_-] \cdot \hat{\vec{n}}$, where $\Delta \phi = 2 \sqrt{r/u}$ is the miscibility gap and $\vec{u} \cdot \hat{\vec{n}}$ is the local normal velocity of the interface [$\hat{\vec{n}}$ is the unit normal point from the $(-)$ phase towards the $(+)$ phase]. Furthermore, Eq. (4), in the absence of flow, leads to the Gibbs-Thomson modification of the coexistence values across a curved interface. All terms in Eqs. (5) and (6) are standard except for the last term on the right-hand side of Eq. (6). Some further insight into the role of this term can be gained by considering the limit of a thin interfacial region. The unit normal to the level sets of constant ϕ is given by $\hat{\vec{n}} = \frac{\vec{\nabla} \phi}{|\vec{\nabla} \phi|}$ so that

$$\mu \vec{\nabla} \phi = |\vec{\nabla} \phi| \, [-K \nabla^2 \phi - r \phi + u \phi^3] \hat{\vec{n}}. \tag{7}$$

The mean curvature of each level set is

$$\kappa = \vec{\nabla} \cdot \hat{\vec{n}} = \vec{\nabla} \cdot \frac{\vec{\nabla} \phi}{|\vec{\nabla} \phi|} = \frac{1}{|\vec{\nabla} \phi|} [\nabla^2 \phi - \vec{\nabla} \vec{\nabla} \phi : \hat{\vec{n}} \hat{\vec{n}}] \tag{8}$$

so that Eq. (7) can be rewritten as

$$\mu \vec{\nabla} \phi = -K \kappa |\nabla \phi|^2 \hat{\vec{n}} + \; [-r \phi + u \phi^3 - K \vec{\nabla} \vec{\nabla} \phi : \hat{\vec{n}} \hat{\vec{n}}] \vec{\nabla} \phi \; . \tag{9}$$

Recall that the surface tension σ is the excess free energy per unit surface area due to the inhomogeneity in ϕ in the interfacial region [27]

$$\sigma = K \int_{-\infty}^{+\infty} dz \left(\frac{d \phi_0}{dz} \right)^2 = \frac{\sqrt{2}}{3} \frac{K^{1/2} r^{3/2}}{u}. \tag{10}$$

In the limit of gently curved interfaces, and when the motion of the interface is slow compared with the local relaxation times of ϕ, the order parameter field ϕ can be approximated by the one-dimensional stationary solution ϕ_0 along the direction normal to the interface. Under these conditions, the term in square brackets in Eq. (9) vanishes. Furthermore, in this limit,

$$\mu \vec{\nabla} \phi \simeq -|\vec{\nabla} \phi|^2 K \kappa \hat{\vec{n}} \simeq -\sigma \kappa \delta(\zeta) \hat{\vec{n}}, \tag{11}$$

with $\zeta = 0$ being the location of the interface and $\delta(x)$ the Dirac delta function. The second equality follows from the definition of the surface tension and by integrating both sides from $\zeta = -\infty$ to ∞. Therefore the new term $\mu \vec{\nabla} \phi$ is zero in the bulk regions and leads to a capillary force at the interfaces. We note at this point that the choice of free energy Eq. (4) is not unique. However, for any reasonable choice of $\mathcal{F}$ that admits interfacial solutions of small width compared to the scale of the structure, the same macroscopic equations will result in the limit $\xi \kappa \to 0$, but with different values of the numerical coefficients.

Finally, the boundary conditions on the order parameter at the walls of the cavity are $\vec{\nabla} \phi \cdot \hat{\vec{n}} = 0$ (see the

Appendix) and $\vec{J}\cdot\hat{\vec{n}}=0$, with $\vec{J}=-M\vec{\nabla}\mu$ the flux of ϕ ($\hat{\vec{n}}$ is the unit normal to the wall). No-slip boundary conditions are applied on the velocity field at the cavity walls: $\vec{v}=0$ at the three walls located at $x=0$, $x=L$, and $y=L$, and $\vec{v}=V_0w(x)\hat{\vec{i}}$ at $y=0$, where $\hat{\vec{i}}$ is the unit vector parallel to the x direction and $w(x)$ is a dimensionless function of x, of order 1, that will be specified later [26]. Hence the wall at $y=0$ is being displaced at a prescribed velocity $V_0w(x)$ to induce the shear flow in the interior of the cavity. With this choice of boundary conditions, the integral of ϕ over the cavity is constant in time. It should also be noted that we do not prescribe the value of ϕ at any wall. Therefore the point of contact between the interface and the walls can move through diffusion of the order parameter near the wall.

We introduce dimensionless variables by scaling the order parameter ϕ by its mean-field equilibrium value $\sqrt{r/u}$, lengths by the mean-field thickness of the interface $\xi=\sqrt{K/r}$, and velocity by the imposed velocity at the boundary V_0. In dimensionless variables, we have

$$\partial_t\phi=-\vec{v}\cdot\vec{\nabla}\phi+\frac{1}{\mathrm{Pe}}\nabla^2\mu, \tag{12}$$

where we have defined a Péclet number $\mathrm{Pe}=V_0\xi/Mr$. The characteristic time has been chosen to be ξ/V_0, the time required for the fluid to be convected a distance of the order of the thickness of the interface (in the absence of capillarity). The Péclet number is the ratio between the diffusive time scale ξ^2/Mr and the convective time scale ξ/V_0. The dimensionless equation of conservation of momentum (for constant viscosity) reads

$$\mathrm{Re}\left[\partial_t\vec{v}+\left(\vec{v}\cdot\vec{\nabla}\right)\vec{v}\right]=-\vec{\nabla}p+\nabla^2\vec{v}+C\mu\vec{\nabla}\phi, \tag{13}$$

where the Reynolds number is $\mathrm{Re}=V_0\xi/\nu$ and C has the form of a capillary number $C=r^2\xi/u\eta V_0=3\sigma/2\eta V_0$.

III. NUMERICAL ALGORITHM

We restrict our analysis to low Reynolds number flows (creeping flows) and set the left-hand side of Eq. (13) equal to zero. Since the flow is incompressible and two dimensional, it is convenient to introduce the stream function ψ,

$$\vec{v}=\vec{\nabla}\times(\psi\hat{\vec{k}})=\frac{\partial\psi}{\partial y}\hat{\vec{i}}-\frac{\partial\psi}{\partial x}\hat{\vec{j}}, \tag{14}$$

where $\vec{v}=v_x\hat{\vec{i}}+v_y\hat{\vec{j}}$ is the fluid velocity in the plane of the cavity and $\hat{\vec{k}}$ is the unit vector in the direction normal to it. By taking the curl of Eq. (13) in the creeping flow limit we obtain

$$\nabla^4\psi-C(\vec{\nabla}\mu\times\vec{\nabla}\phi)\cdot\hat{\vec{k}}=0. \tag{15}$$

Since $\mu=-\nabla^2\phi+f'(\phi)$, we finally find

$$\nabla^4\psi+C\left[\vec{\nabla}(\nabla^2\phi)\times\vec{\nabla}\phi\right]\cdot\hat{\vec{k}}=0. \tag{16}$$

Therefore the solution of the flow field entails solving a biharmonic equation for the stream function [Eq. (16)], subject to the boundary conditions that $\psi=0$ at all boundaries, $\partial\psi/\partial n=0$ at the boundaries at $x=0, x=L$, and $y=L$, and $\partial\psi/\partial n=w(x)$ at $y=0$ (L is here the dimensionless side of the cavity).

Concerning the equation for the order parameter Eq. (12), we follow Ref. [28] and use a backward implicit method

$$\mathrm{Pe}\frac{\phi(t+\Delta t)-\phi(t)}{\Delta t}+\mathrm{Pe}\vec{\nabla}\cdot[\vec{v}(t)\phi(t+\Delta t)]$$
$$=-\mathcal{L}\phi(t+\Delta t)+\nabla^2\phi^3(t+\Delta t), \tag{17}$$

with $\mathcal{L}=\nabla^4+\nabla^2$. Note that the convective term is kept in conservative form and that we use the velocity at time t. Although one could in principle use $\vec{v}(t+\Delta t)$ in Eq. (17), this would result in a more complex iterative procedure. If the iterative procedure to be described below converges, the solution is (up to roundoff error) independent of this choice. An "outer iteration" is defined as

$$\phi(t+\Delta t)\simeq\phi_{k+1}=\phi_k+\delta_k \quad\text{with}\quad \phi_0=\phi(t)\ . \tag{18}$$

Substituting $\phi(t+\Delta t)$ in Eq. (18), linearizing in the correction δ_k, and rearranging terms, we obtain

$$\left[\mathcal{L}+\frac{\mathrm{Pe}}{\Delta t}-3\nabla^2\phi_k^2-6\vec{\nabla}\phi_k^2\cdot\vec{\nabla}-3\phi_k^2\nabla^2\right]\delta_k$$
$$+\mathrm{Pe}\vec{\nabla}\cdot(\vec{v}_k\delta_k)=-\mathcal{L}\phi_k+\nabla^2\phi_k^3-\frac{\mathrm{Pe}(\phi_k-\phi_0)}{\Delta t}$$
$$-\mathrm{Pe}\vec{\nabla}\cdot(\vec{v}_k\phi_k). \tag{19}$$

The right-hand side of this equation is the outer residual, or $r^{\phi}_{\mathrm{outer},k}$. The velocity $\vec{v}_k$ is obtained by solving Eq. (16) for the stream function with $\phi=\phi_k$ and by substituting the solution into Eq. (14). The outer iteration converges when $\|\,r^{\phi}_{\mathrm{outer},k}\,\|\to 0$ with, simultaneously, $\|\,\delta_k\,\|\to 0$. When convergence is achieved, the original Eq. (17) is satisfied identically and $\phi(t+\Delta t)$ is taken to be the last iterate.

In practice, it is convenient to set up an additional "inner" iteration to solve Eq. (19) defined as

$$\delta_k\simeq\delta_{k,m+1}=\delta_{k,m}+\eta_m. \tag{20}$$

Substitution of Eq. (20) into Eq. (19) and linearizing with respect to η_m yields

$$\left[\mathcal{L}+\frac{\mathrm{Pe}}{\Delta t}+\mathrm{Pe}\ \vec{v}_k\cdot\vec{\nabla}-3\phi_k^2\nabla^2-6\phi_k\nabla^2\phi_k\right]\eta_m$$

$$=r^{\phi}_{\mathrm{outer(k)}}-\left[\mathcal{L}+\frac{\mathrm{Pe}}{\Delta t}+\mathrm{Pe}\ \vec{v}_k\cdot\vec{\nabla}-3\phi_k^2\nabla^2-6\phi_k\nabla^2\phi_k\right]\delta_{k,m}, \quad (21)$$

where the right-hand side is the inner residual $r^{\phi}_{\mathrm{inner},m}$. We next simplify the left-hand side by neglecting the term $\mathrm{Pe}\,\vec{v}_k\cdot\vec{\nabla}\eta_m$ and by approximating the terms $3\phi_k^2\nabla^2\eta_m$ and $-6\phi_k\nabla^2\phi_k$ by average values as follows:

$$a=1-3\langle\phi_k^2\rangle, \qquad b=\frac{\mathrm{Pe}}{\Delta t}-6\langle\phi_k\nabla^2\phi_k\rangle, \quad (22)$$

where $\langle\,\rangle$ denotes a spatial average over the cavity. Equation (21) is now

$$\left[\nabla^4+a\nabla^2+b\right]\eta_m=r^{\phi}_{\mathrm{inner},m}. \quad (23)$$

Equation (23) has now the same functional form as Eq. (16) and both are solved with the aid of a fast biharmonic solver [28]. In practice, for k fixed, Eq. (23) is iterated over m until convergence is achieved and hence δ_k is determined. Following [28], the convergence criterion used for the inner iteration is given by

$$\frac{\|r_{\mathrm{inner},m}\|}{\|r_{\mathrm{outer},k}\|}\le\alpha\left(\frac{\|r_{\mathrm{outer},k}\|}{\|r_{\mathrm{outer},0}\|}\right)^{\beta}, \quad (24)$$

with $\alpha=0.1$ and $\beta=0.5$. Next ϕ_{k+1} is computed and used to obtain $\vec{v}_{k+1}$ by solving Eqs. (16) and (14). A new inner iteration is then used to find δ_{k+1} for the new velocity field $\vec{v}_{k+1}$. This procedure is repeated until the outer iteration converges. The convergence criterion used for the outer iteration is

$$\max[||\delta_k||,||r_{\mathrm{outer}}(k)||]\le\epsilon_{\mathrm{rel}}[||\phi(k)||]+\epsilon_{\mathrm{abs}}\ , \quad (25)$$

where ϵ_{rel} and ϵ_{abs} are the relative and absolute error norms, chosen here to be 0.1 and 10^{-4}, respectively.

IV. RESULTS

We have used the algorithm described in the preceding section to track the evolution of an active interface in the configuration described in Sec. II. Unless otherwise noted, the results presented below correspond to a square, two-dimensional cavity of dimensionless side $L=100$. The solution of the biharmonic equation is done on a uniform, square grid, with $N=256$ nodes in each direction. The time step used for the integration is $\Delta t=0.1$. At $t=0$, $\phi=-1$ for $0\le x\le L, 0\le y\le L/2$, and $\phi=1$ in the remainder of the cavity. This corresponds to an initially flat interface parallel to the direction of shear (we define the interface location to be the position of the level set $\phi=0$). Examples of evolution of the interface at various times are shown in Figs. 1 and 2. The stream function corresponding to Fig. 2 is shown in Fig. 3. The interfacial perimeter length S is computed by adding the length of all the line segments connecting grid nodes that separate regions of ϕ of different sign. The contribution of each of these line segments is equal to the grid spacing h or $\sqrt{2}h$ depending on whether the line segment is oriented parallel or diagonal to the grid lines, respectively.

We first compare our numerical results with the classical calculation of the stretching of a material line advected by the flow. In this case, it is possible to obtain analytically a Galerkin approximation to the flow in the cavity [29] and then to compute numerically the interfacial perimeter length of a material line passively advected by the flow. We note that in the analytic calculation given in Ref. [29] the discontinuity in velocity at the cor-

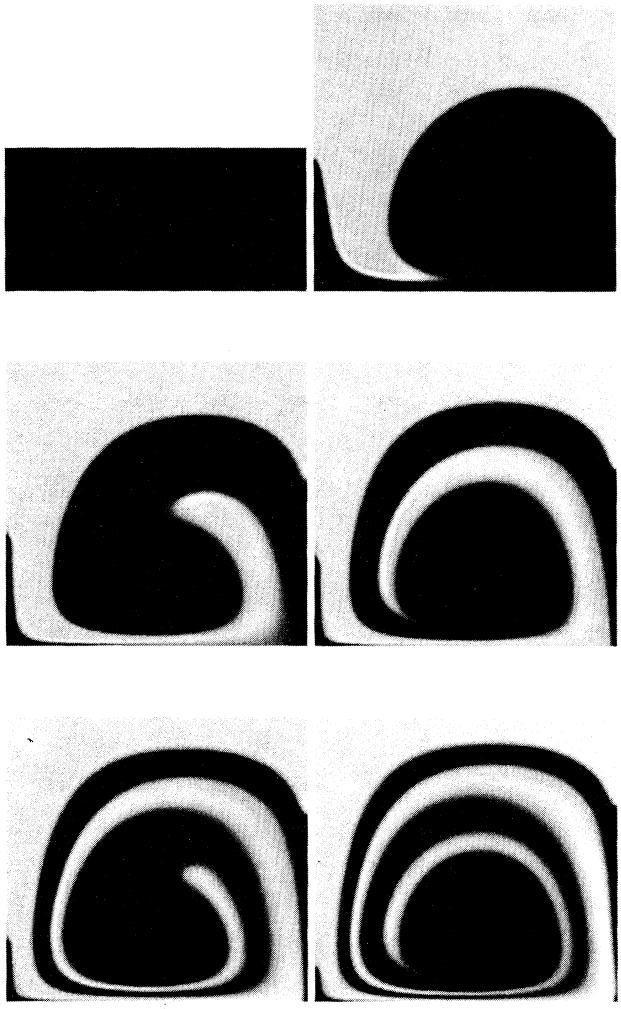

FIG. 1. Instantaneous values of the order parameter ϕ (in gray scale) as a function of time for $C=0.1$ and $\mathrm{Pe}=10^3$. The configurations shown (from top to bottom and left to right) correspond to intervals of $\Delta t=500$, starting from the initial configuration.

ners of the moving plate is avoided [26]. The flow field is obtained by using a single-mode Galerkin approximation and by solving self-consistently for both the amplitude of the mode and the tangential velocity of the moving plate. The solution found is [29]

$$w(x) = \gamma x^2(1-x)^2, \tag{26}$$

with $\gamma = 21$. The corresponding velocity field in the cavity is given by

$$\begin{aligned} v_x &= \gamma x^2(1-x)^2\{A_2[(\delta_1^2+\delta_2^2)/\delta_1]\ \sinh(\delta_1 y)\sin(\delta_2 y) \\ &\quad +B_1[\delta_2\sinh(\delta_1 y)\cos(\delta_2 y) \\ &\quad +\delta_1\cosh(\delta_1 y)\sin(\delta_2 y)]\}, \\ v_y &= 2\gamma x(1-x)(1-2x)[A_2\cosh(\delta_1 y)\sin(\delta_2 y) \\ &\quad +\ B_1\sinh(\delta_1 y)\sin(\delta_2 y) \\ &\quad +B_2\sinh(\delta_1 y)\cos(\delta_2 y)]\ , \end{aligned} \tag{27}$$

with $\delta_1 = 4.15$, $\delta_2 = 2.286$,

$$A_2 = -\frac{\delta_1\sinh\delta_1\sin\delta_2}{\delta_2^2\sinh^2\delta_1 - \delta_1^2\sin^2\delta_2},$$

$$B_1 = \frac{\delta_1\cosh\delta_1\sin\delta_2 - \delta_2\sinh\delta_1\cos\delta_2}{\delta_2^2\sinh^2\delta_1 - \delta_1^2\sin^2\delta_2},$$

and $B_2 = -A_2\delta_2/\delta_1$. The boundary condition in Eq. (26) is also used in all our numerical calculations.

The velocity field in Eq. (27) is then used to calculate numerically the stretching of a passive interface by following the motion of the material line originally located at $\phi = 0$. In Fig. 4 the interface stretching thus calculated is compared with the results given by our model with $C = 0$. The agreement is good up to $S(t)/S(t=0) \approx 5$. The local normal velocity of the interface has two contributions: local advection due to the induced flow in the cavity and flow resulting from relaxation of the or-

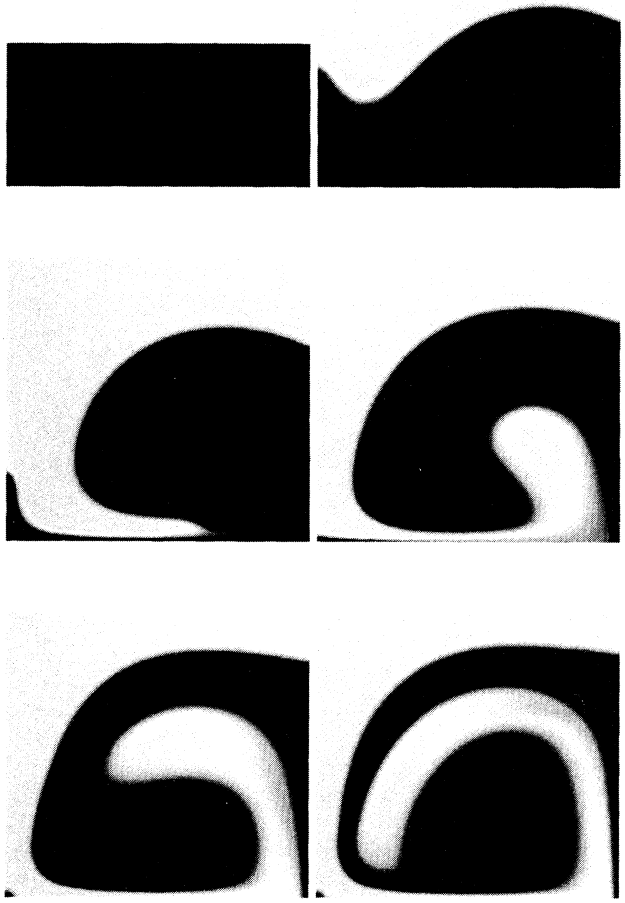

FIG. 2. Instantaneous values of the order parameter ϕ (in gray scale) as a function of time for $C = 1$ and $\mathrm{Pe} = 10^3$. The configurations are shown for the same times as in Fig. 1.

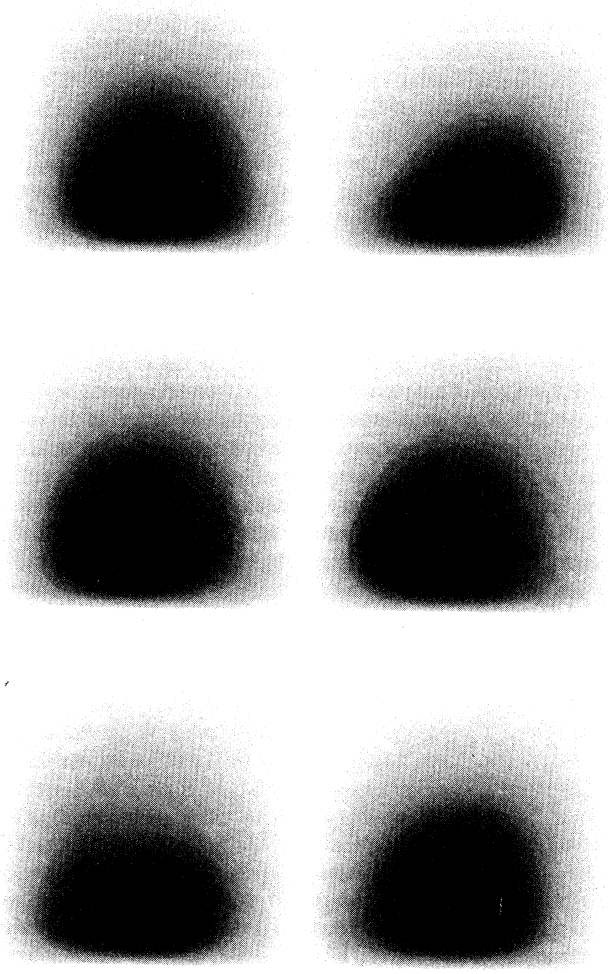

FIG. 3. Stream function (in gray scale) corresponding to the configurations shown in Fig. 2. The maximum values of the stream function are 9.50, 9.34, 9.19, 8.53, 8.81, and 9.57, respectively. The minimum value of the stream function is at the boundary and equals zero.

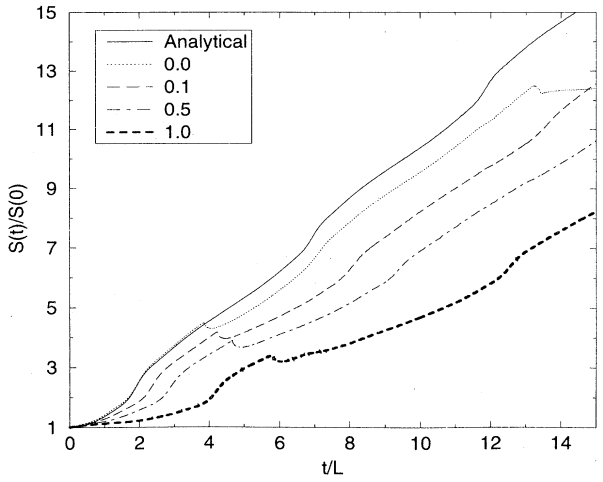

FIG. 4. Interfacial stretch $S(t)/S(t=0)$ as a function of time for various values of the capillary number C and $\mathrm{Pe} = 10^3$. The solid line is the approximate analytic calculation described in the text for the passive advection of a material line ($C = 0$ and $\mathrm{Pe} \to \infty$). The other curves shown correspond to $C = 0$ (passive interface), $C = 0.1$, $C = 0.5$, and $C = 1$. We note that the ratio $t/L = t^* V_0/L^*$, where we have denoted dimensional variables with an asterisk. The latter quantity is normally the unit of time employed in classical macroscopic calculations.

der parameter to maintain its local equilibrium value as a function of the local curvature of the interface (Gibbs-Thomson effect). At later times, the curvature of the interface increases and the latter contribution becomes significant. This is why the interface stretching given by our solution is smaller, even for $C = 0$, than the stretching that follows from the passive advection of a material line.

Figure 4 also shows the interfacial stretching for different values of the capillary number C. With increasing C, the slope of the curve decreases. Capillarity acts to reduce the interfacial deformation and hence counteracts the effect of the imposed flow on the interface displacement. As a consequence, for example, the interfacial shape shown in Fig. 2 ($C = 1$) is blunter than that shown in Fig. 1 ($C = 0.1$) at comparable times.

Figure 5(a) shows the interfacial stretching as a function of time for constant C and different values of the Péclet number. The interfacial length S increases roughly linearly with time, until it reaches a maximum at roughly $S_{\max}$, a value that depends on Pe. At this point, the microstructure coarsens since further stretching by the flow is balanced by diffusion of the order parameter. Whereas the diffusive contribution in Eq. (12) is proportional to Pe^{-1}, the chemical potential μ is of the order of $\sigma\kappa$, which becomes large as the scale of the microstructure decreases. At even longer times (which we will not address here) and for small values of Pe, S further decreases with time as the system evolves into a stationary state in which a strip of one phase rotates inside the other, with an axis of rotation located approximately at

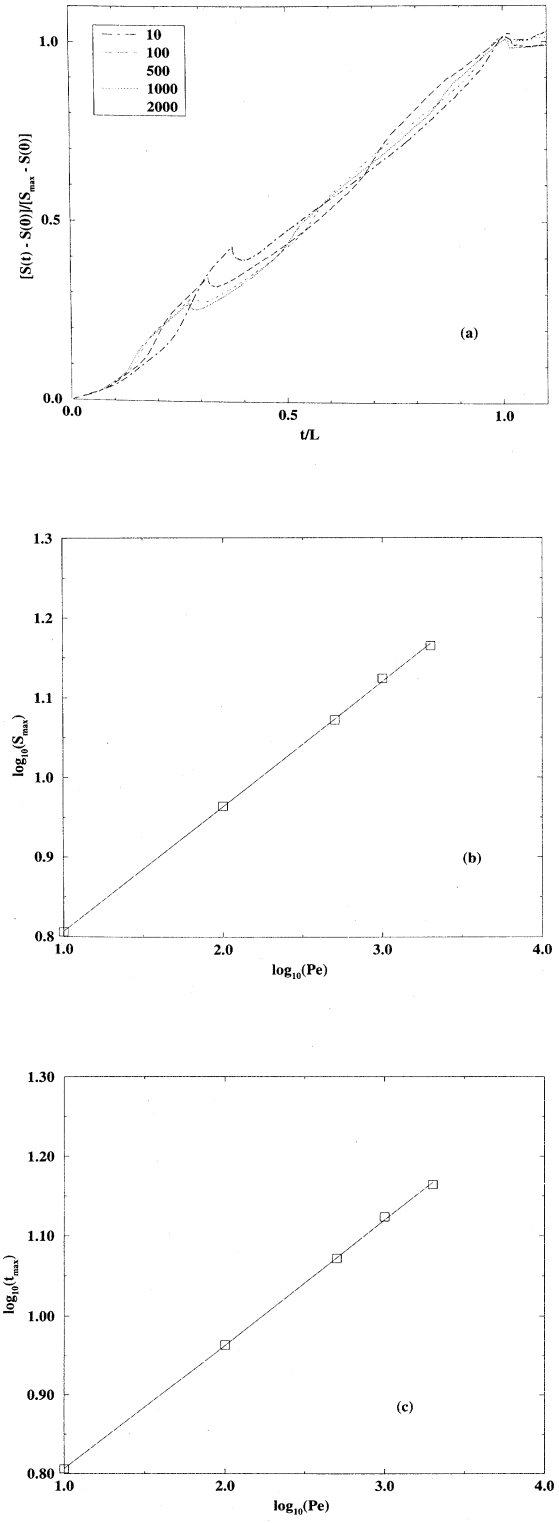

FIG. 5. (a) Scaled interfacial stretch $S(t/t_{\max})/S_{\max}$ for $C = 0.1$ and the values of the Péclet number shown. The value of $S_{\max}$ is the largest interfacial stretch (reached at time $t_{\max}$ for a given set of parameters, when the microstructure begins to coarsen). The dependence of $S_{\max}$ and $t_{\max}$ on Pe is shown in (b) and (c) respectively. The solid lines in (b) and (c) have a slope of approximately 0.15.

the point where the velocity of the fluid vanishes. This asymptotic stationary state is known for this type of flow and results in poor mixing of the two phases. In Fig. 5(a) we have scaled S by $S_{\max}$ and t by $t_{\max}$, the time that corresponds to $S_{\max}$. In Figs. 5(b) and 5(c), the dependence of $S_{\max}$ and $t_{\max}$ with Pe is shown. In the limit of Pe $\to \infty$, the problem effectively reduces to that of advecting the interface separating two immiscible fluids. However, Eq. (12) becomes hyperbolic and the numerical algorithm must be modified. In practice, we are able to achieve convergence in the cavity configuration studied for Pe ≤ 2000.

Finally, we have analyzed the dependence of the interfacial stretch S on the size of the cavity L. For early times, S grows linearly in time (see, for example, Fig. 5), with a slope that is proportional to $1/L$. The reason for this is that, at constant velocity of the top plate, the resulting shear is inversely proportional to the size of the cavity. The maximum value of S also grows linearly in time for sufficiently large L ($L > 75$). Since the smallest length scale in the system is effectively determined by the values of the Péclet and capillary numbers, the scale of the structure is expected to be proportional to the system size, at constant values of the other fluid parameters.

In summary, we have introduced a mesoscopic description of a two-phase fluid to study interface stretching induced by an externally imposed shear flow. The algorithm allows us to track interfacial stretchings that are much higher than those obtained with previous approaches and opens the possibility of quantitative studies of the resulting microstructure. The validity of the algorithm discussed is restricted to low Reynolds number flows, but the method can in principle be generalized to other situations.

ACKNOWLEDGMENTS

This work is supported by the U.S. Department of Energy, Contract No. DE-FG05-95ER14566, and also in part by the Supercomputer Computations Research Institute, which is partially funded by the U.S. Department of Energy, Contract No. DE-FC05-85ER25000.

APPENDIX: DISSIPATION INEQUALITY

We define the total energy E of the fluid as

$$E(\phi,\vec{g}) = \mathcal{F}(\phi) + \frac{1}{2}\int \frac{g^2}{\rho} dA \ ,$$

where $\vec{g} = \rho\vec{v}$ is the momentum density. The rate of change of the total energy can be obtained as

$$\frac{dE}{dt} = \int \frac{\delta E}{\delta\phi}\frac{\partial\phi}{\partial t} dA + \int \frac{\delta E}{\delta\vec{g}} \cdot \frac{\partial\vec{g}}{\partial t} dA$$
$$= \int \mu \frac{\partial\phi}{\partial t} dA + \int \frac{\partial\phi}{\partial t}\vec{\nabla}\phi\cdot\hat{\vec{n}} dl + \int \vec{v}\cdot\frac{\partial\vec{g}}{\partial t} dA,$$

where $\hat{\vec{n}}$ is the outward pointing normal to the cavity and dl is the element of perimeter length of the cavity. By using Eqs. (2)–(4) and (6), we find

$$\frac{dE}{dt} = \int \mu\left(M\nabla^2\mu - \vec{v}\cdot\nabla\phi\right) dA$$
$$+ \int \vec{v}\cdot\left(2\eta\vec{\nabla}\cdot D - \vec{\nabla}p + \mu\vec{\nabla}\phi\right) dA$$
$$+ \int \frac{\partial\phi}{\partial t}\vec{\nabla}\phi\cdot\hat{\vec{n}}\, dl. \qquad \text{(A1)}$$

The first term on the right-hand side can be rewritten by using the identity $\mu\nabla^2\mu = \vec{\nabla}\cdot(\mu\vec{\nabla}\mu) - (\vec{\nabla}\mu)^2$ and the divergence theorem as

$$\int \mu\nabla^2\mu\, dA = \int \mu(\vec{\nabla}\mu\cdot\hat{\vec{n}}) dl - \int (\vec{\nabla}\mu)^2 dA.$$

The third and fourth terms on the right-hand side of Eq. (A1) can be rewritten by using the identities $\vec{v}\cdot(\vec{\nabla}\cdot D) = \vec{\nabla}\cdot(D\cdot\vec{v}) - D{:}D$ and $\vec{v}\cdot\vec{\nabla}p = \vec{\nabla}\cdot(p\vec{v}) - p(\vec{\nabla}\cdot\vec{v}) = \vec{\nabla}\cdot(p\vec{v})$, where the incompressibility condition was used in the last step. Then using the divergence theorem again

$$\int \vec{v}\cdot(\vec{\nabla}\cdot D)\, dA = \int (D\cdot\vec{v})\cdot\hat{\vec{n}}\, dl - \int D{:}D\, dA$$

and

$$\int \vec{v}\cdot\vec{\nabla}p\, dA = \int p\vec{v}\cdot\hat{\vec{n}}\ dl.$$

Finally, by using the boundary conditions

$$\vec{\nabla}\phi\cdot\hat{\vec{n}} = 0, \quad \vec{\nabla}\mu\cdot\hat{\vec{n}} = 0, \quad \vec{v} = \vec{0}, \qquad \text{(A2)}$$

we have the dissipation inequality

$$\frac{dE}{dt} = -M\int (\vec{\nabla}\mu)^2 dA - 2\eta\int D{:}D\, dA \leq 0\ .$$

Therefore, in the absence of shear, the natural boundary conditions to consider in order to ensure that the energy decreases monotonically are given by Eq. (A2).

[1] J. Ottino, *The Kinematics of Mixing, Cambridge Texts in Applied Mathematics* (Cambridge University Press, New York, 1989).

[2] J. D. Gunton, M. San Miguel, and P. S. Sahni, in *Phase Transitions and Critical Phenomena*, edited by C. Domb and J. Lebowitz (Academic, London, 1983), Vol. 8.

[3] J. S. Langer, in *Directions in Condensed Matter Physics*, edited by G. Grinstein and G. Mazenko (World Scientific, Philadelphia, 1986), p. 165.

[4] G. Caginalp, in *Applications of Field Theory to Statistical Mechanics*, edited by L. Garrido, Lecture Notes in Physics Vol. 216 (Springer-Verlag, Berlin, 1985), p. 216.

[5] G. Caginalp and P. C. Fife, Phys. Rev. B **33**, 7792 (1986).
[6] S.-L. Wang *et al.*, Physica D **69**, 189 (1993).
[7] B. Grossmann, K. R. Elder, M. G. Grant, and J. M. Kosterlitz, Phys. Rev. Lett. **71**, 3323 (1993).
[8] P. C. Hohenberg and B. I. Halperin, Rev. Mod. Phys. **49**, 435 (1977).
[9] E. D. Siggia, B. I. Halperin, and P. C. Hohenberg, Phys. Rev. B **13**, 2110 (1976).
[10] A. Onuki and K. Kawasaki, Ann. Phys. (N.Y.) **121**, 456 (1979).
[11] A. Onuki, K. Yamazaki, and K. Kawasaki, Ann. Phys. (N.Y.) **131**, 217 (1981).
[12] E. Helfand and G. H. Fredrickson, Phys. Rev. Lett. **62**, 2468 (1989).
[13] K. Kawasaki and T. Ohta, Physica A **118**, 175 (1983).
[14] T. Koga and K. Kawasaki, Phys. Rev. A **44**, R817 (1991).
[15] M. E. Gurtin, D. Polignone, and J. Viñals, Math. Models Methods Appl. Sci. (to be published).
[16] J. Hyman, Physica D **12**, 396 (1984).
[17] E. Oran and J. Boris, *Numerical Simulations of Reactive Flows* (Elsevier, New York, 1987).
[18] C. W. Hirt and B. D. Nichols, J. Comput. Phys. **39**, 201 (1981).
[19] S. O. Unverdi and G. Trygvasson, J. Comput. Phys. **100**, 25 (1992).
[20] Q. Shi and H. Haj-Hariri, in *Proceedings of the 32nd Aerospace Sciences Meeting* (AIAA, Washington, 1994).
[21] H. Haj-Hariri, Q. Shi, and A. Borhan, Phys. Fluids **6**, 2555 (1994).
[22] D. Bigg and S. Middleman, Ind. Eng. Chem. Fundam. **13**, 184 (1974).
[23] J. Cahn, Acta Metall. **9**, 795 (1961).
[24] P. Flory, *Principles of Polymer Chemistry* (Cornell University Press, Ithaca, 1967).
[25] K. Binder, Phys. Rev. A **29**, 341 (1984).
[26] The natural boundary condition $\vec{v} = V_0 \hat{\vec{i}}$ at $y = 0$ leads to a discontinuity in the velocity at the boundary. Within a classical macroscopic description, the discontinuity in the tangential velocity leads to a divergence in the Newtonian stress tensor as the corner is approached. At a miscrocopic level, however, the fluid near the wall slips and the microscopic stress tensor remains finite. We have not addressed this issue in detail for the mesoscopic formulation that we use in this paper. In order to avoid the issue, as well as to be able to compare our numerical results with previous semianalytic work, we have chosen an (unphysical) velocity profile at the bottom plate that goes smoothly to zero as both corners are approached.
[27] J. Rowlinson and B. Widom, *Molecular Theory of Capillarity* (Clarendon, Oxford, 1982).
[28] P. Bjorstad *et al.*, *Elliptic Problem Solvers II* (Academic, New York, 1984).
[29] R. Chella and J. M. Ottino, I&EC Fund. **24**, 170 (1985).

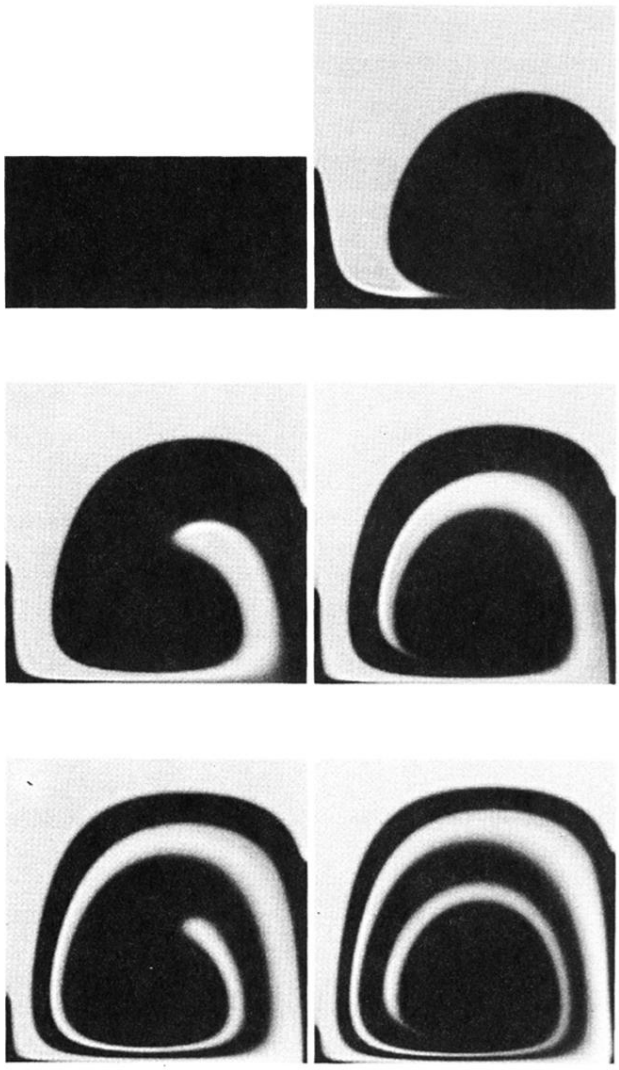

FIG. 1. Instantaneous values of the order parameter ϕ (in gray scale) as a function of time for $C = 0.1$ and $\mathrm{Pe} = 10^3$. The configurations shown (from top to bottom and left to right) correspond to intervals of $\Delta t = 500$, starting from the initial configuration.

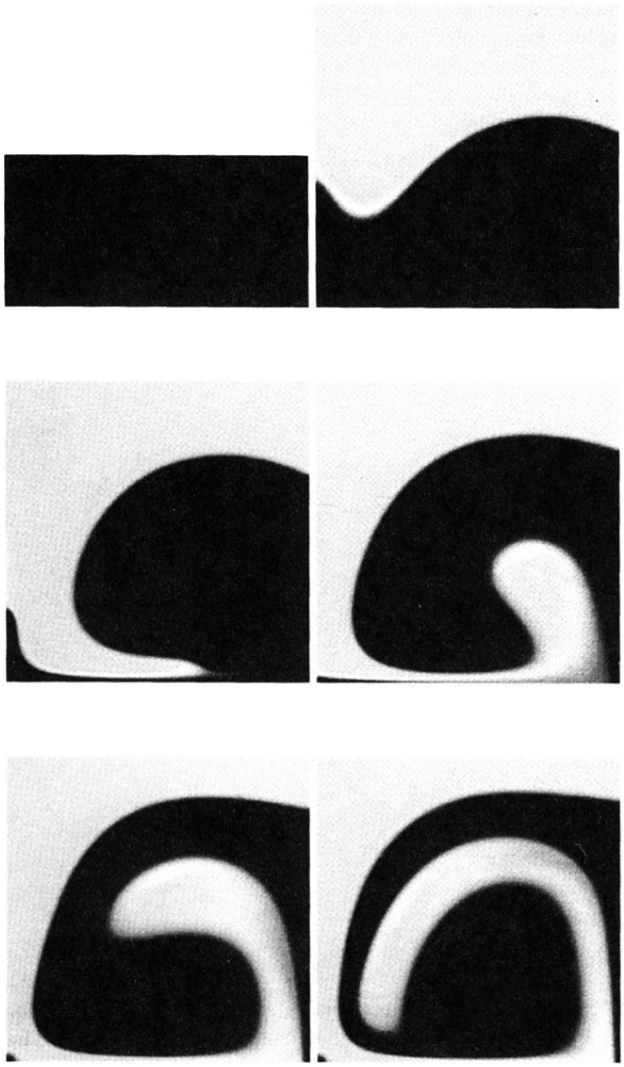

FIG. 2. Instantaneous values of the order parameter ϕ (in gray scale) as a function of time for $C = 1$ and $\mathrm{Pe} = 10^3$. The configurations are shown for the same times as in Fig. 1.

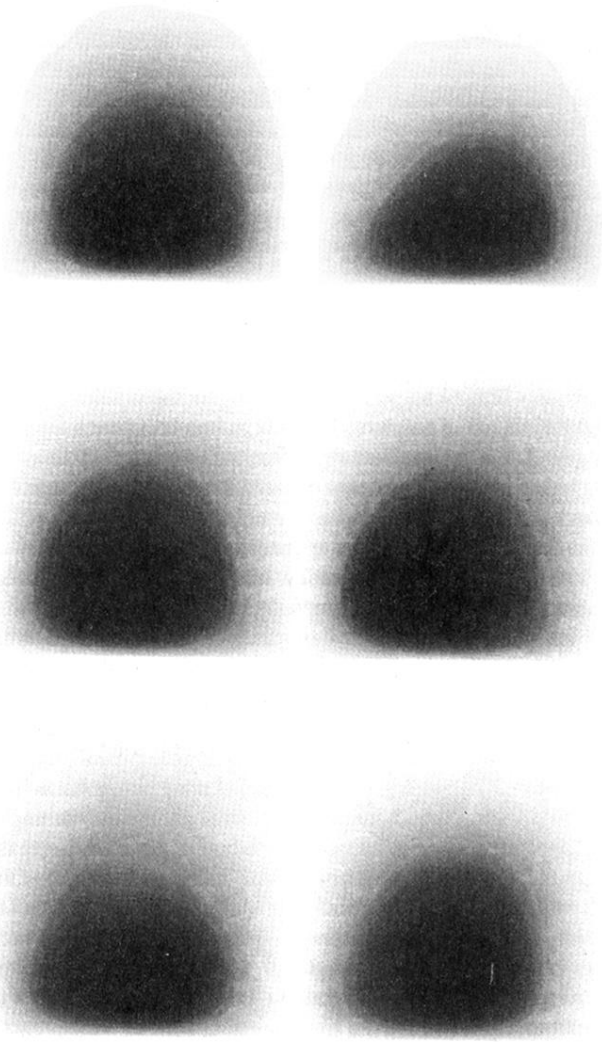

FIG. 3. Stream function (in gray scale) corresponding to the configurations shown in Fig. 2. The maximum values of the stream function are 9.50, 9.34, 9.19, 8.53, 8.81, and 9.57, respectively. The minimum value of the stream function is at the boundary and equals zero.